

# ZeST: an LLM-based Zero-Shot Traversability Navigation for Unknown Environments

Shreya Gummadi<sup>1†</sup>, Mateus V. Gasparino<sup>1†</sup>, Gianluca Capezzuto<sup>2</sup>, Marcelo Becker<sup>2</sup>, and Girish Chowdhary<sup>1</sup>

**Abstract**—The advancement of robotics and autonomous navigation systems hinges on the ability to accurately predict terrain traversability. Traditional methods for generating datasets to train these prediction models often involve putting robots into potentially hazardous environments, posing risks to equipment and safety. To solve this problem, we present ZeST, a novel approach leveraging visual reasoning capabilities of Large Language Models (LLMs) to create a traversability map in real-time without exposing robots to danger. Our approach not only performs zero-shot traversability and mitigates the risks associated with real-world data collection but also accelerates the development of advanced navigation systems, offering a cost-effective and scalable solution. To support our findings, we present navigation results, in both controlled indoor and unstructured outdoor environments. As shown in the experiments, our method provides safer navigation when compared to other state-of-the-art methods, constantly reaching the final goal.

**Index Terms**—Field Robots, Vision-Based Navigation, Semantic Scene Understanding.

## I. INTRODUCTION

The development of autonomous navigation systems is a cornerstone of robotics, with terrain traversability prediction being a critical component [1], [2], [3], [4], [5]. Traversability prediction refers to the ability of a robot to assess whether a given terrain is passable or poses risks to its operation. This capability is essential for a wide range of applications, including planetary exploration, disaster response, and autonomous vehicles. However, accurately predicting terrain traversability presents significant challenges due to the diversity and unpredictability of real-world environments [1].

Traditional approaches to traversability prediction often rely on heuristic-based methods [6]. These methods require domain expertise and extensive trial-and-error processes to convert sensor data into actionable navigation insights [7]. While effective in controlled or well-defined settings, heuristic-based methods struggle to generalize to unknown or dynamic terrains, limiting their applicability in real-world scenarios. Another common solution involves supervised learning using neural networks trained on labeled datasets [8], [9]. Although this approach has shown promise in improving prediction accuracy, it necessitates labor-intensive manual labeling and expert annotations, making it both costly and time-consuming.

A more recent trend involves learning from experience, where robots gather data through direct interaction with their

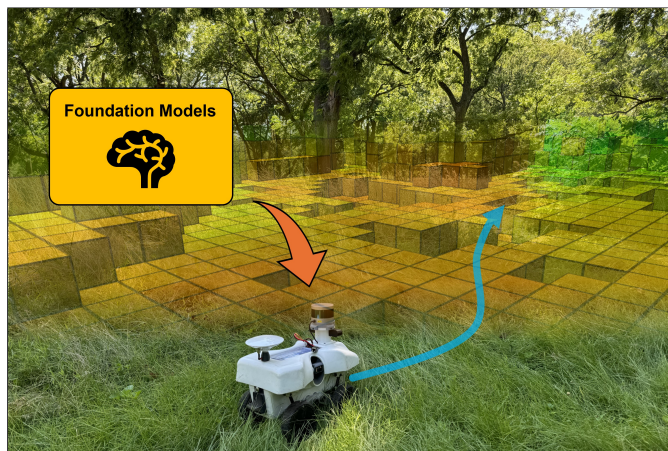


Fig. 1: We present ZeST, a Zero-Shot Traversability navigation method that is able to navigate in unknown environments without the need of fine-tuning.

environment. This approach eliminates the need for pre-labeled datasets and allows robots to adapt to specific terrains by learning from their own experiences. However, this method introduces safety concerns as robots must operate in potentially hazardous environments during the data collection phase. For instance, deploying robots in disaster zones or rugged terrains for training purposes risks damaging equipment and endangering operational integrity.

### A. Contributions

To address these challenges, we present **ZeST** (Zero-Shot Traversability), a novel framework that leverages Large Language Models (LLMs) for real-time terrain traversability prediction. ZeST eliminates the need for physical interaction with the environment during training by leverage the reasoning capabilities of multimodal LLMs to infer terrain properties based on contextual information rather than direct experience, which enables robots to generate traversability maps without exposing themselves to unsafe conditions. For example, given the characteristics of our robot, an LLM can analyze the traversability levels of certain parts of the terrain to estimate navigational costs for a robot.

To address prediction variability inherent in LLMs, ZeST models traversability estimates as samples from a Normal Inverse Gamma (NIG) distribution, explicitly capturing both aleatoric and epistemic uncertainties. This probabilistic approach enables ZeST to build coherent global maps of navigational costs while quantifying uncertainty.

To reduce the cost of querying LLMs during deployment, ZeST maintains a dynamic global map that accumulates observations as the robot explores, minimizing repeated inference.

<sup>†</sup> These authors contributed equally to this work.

<sup>1</sup>Field Robotics Engineering and Science Hub (FRESH), Illinois Autonomous Farm, University of Illinois at Urbana-Champaign (UIUC), IL

<sup>2</sup>Mobile Robotics Group, São Carlos School of Engineering, University of São Paulo (EESC-USP), São Carlos, SP, Brazil

The publication was written prior to Mateus V. Gasparino joining Amazon. Contact: {gummadi4, girishc}@illinois.edu

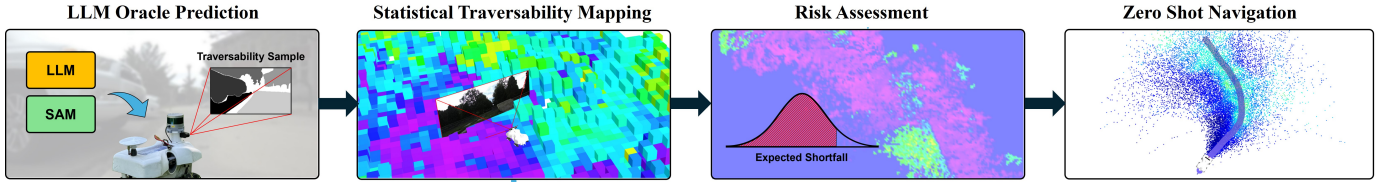


Fig. 2: Overview of the proposed zero-shot navigation pipeline. (1) **LLM Oracle Prediction**: LLM and SAM generate traversability samples. (2) **Statistical Traversability Mapping**: Samples are fused into a probabilistic map. (3) **Risk Assessment**: Navigation risk is quantified via expected shortfall. (4) **Zero-Shot Navigation**: The robot navigates unfamiliar environments using the risk-aware map.

Real-world experiments show that ZeST improves navigational success rates compared to state-of-the-art approaches.

To evaluate our method’s performance, we deploy our system in real-world environments and compare ZeST against state-of-the-art methods for terrain traversability prediction. Our results demonstrate that ZeST improves overall navigational success rates, showcasing its potential as a robust solution for autonomous navigation.

## II. RELATED WORK

Recently, with the advance of Large Language Models (LLM), works on **zero-shot traversability** and/or affordance prediction have emerged [10], [11], [12], [13], [14], [15], [16], [17]. The advancements in LLMs have paved the way for novel approaches to provide actionable predictions that can be used by robotic embodiments. LLMs and Vision Language Models (VLMs) have demonstrated remarkable capabilities in generalization across various domains, including zero-shot classification, semantic visual understanding, and logical reasoning [18], [19], [20], [21], [22], [23], [24], [25]. These models have shown promise in tasks related to embodied vision language navigation and open vocabulary manipulation, suggesting potential applications in perceiving and reasoning about complex environments during autonomous navigation.

For instance, [13] demonstrated how LLMs and VLMs have the capabilities to guide a robot’s exploration to search for user-defined objectives, which can be entered in the form of texts. In this work, they use a Large Language Model (LLM) to parse the user-defined goal into a list of goals, while a VLM is used to guide the robot towards these locations. [14] presents a very similar approach that uses an LLM to decompose navigation instructions into a series of tasks executed by an action-aware navigation policy. Unlike these works, [15] demonstrates the fusion of mapping creation by using VLM features, which averages the output features projected with the help of depth maps. Using this 3D feature map, a language encoder can be used to highlight and understand spatial references relative to landmarks. Similarly, [14] employed an LLM to decompose navigation instructions into a series of tasks executed by an action-aware policy.

However, the application of large VLMs to mobile robot navigation faces several challenges. The substantial computational requirements of these models often exceed the capabilities of onboard processors typically found on robots. Additionally, variable response times of VLMs can take many seconds to be processed, making the use of such methods

unsuitable for real-time safety-critical tasks such as collision avoidance. To address some of these limitations, CoNVOI [17] presents a method that queries these large models to choose between path proposals, which is then executed by the robot. Using a classical LiDAR-based obstacle avoidance, this method is able to alleviate the problem of high latency in the predictions, providing an autonomous navigation for mobile robots. However, these methods are still in the early stages of deployment and are limited to simpler environments where there is not much noise. In addition, prediction noise from these large models is often neglected, which can be risky for robot deployment in real environments. Despite these challenges, the potential of LLMs and VLMs in enhancing robotic navigation through improved environmental understanding and reasoning capabilities remains a promising area of research.

## III. SYSTEM DESIGN

ZeST, illustrated in Fig. 1, is a modular navigation system based on traversability estimation for unstructured and unknown environments. The core objective of ZeST is to enable autonomous robots to navigate safely and efficiently in challenging terrains without requiring prior knowledge or extensive data collection. By leveraging the reasoning capabilities of LLMs and integrating them with probabilistic frameworks, ZeST provides a robust solution for real-time terrain analysis. The system is designed to operate in a modular fashion, allowing seamless integration of its components across diverse robotic platforms and environmental conditions, including multi-modal data processing, uncertainty modeling, and global map construction.



Fig. 3: Example of a prompt used in our work. It gives details about the robotic platform and references for the latent traversability values.

In this section, we detail the architecture and key components of ZeST, highlighting how each module contributes to the overall functionality of the system.

1) *Mask Generation*: An important step in ZeST involves extracting traversability information from LLMs. Currently, LLMs lack explicit traversability prediction capabilities, and in this work, we aim to investigate the zero-shot abilities of large language models to provide useful information for robotics navigation. To achieve this, we implement an intermediary step that pre-processes input images before querying the multimodal LLM on a location by location basis.

To query an image using multimodal LLMs, we highlight areas of the image that are likely to have similar traversability values. This segmentation is based on visual similarity, under the assumption that pixels with similar visual content should correspond to similar traversability values. Given an RGB image, we utilize off-the-shelf models such as the Segment Anything Model (SAM) [26] and the superpixel approach Simple Linear Iterative Clustering (SLIC) [27] to automatically generate masks. These masks segment the image into distinct regions, each representing a meaningful part of the environment. The use of SAM and SLIC is motivated by their efficiency, effectiveness, and ability to produce high-quality segmentation results suitable for downstream tasks involving LLMs.

Given the set of masks generated by SAM or SLIC, we assign each mask a unique identifier ranging from 1 to  $N$ , where  $N$  is the total number of masks in the image. These identifiers are visually marked on the corresponding regions of the image to create a numbered version of the input. This numbering process ensures that each region can be distinctly referenced and analyzed by large multimodal models (LLMs). By associating each mask with a unique number, the LLMs can provide region-specific outputs, such as traversability predictions or semantic interpretations, enabling fine-grained analysis of the environment.

2) *Querying the Large Language Model*: To analyze the segmented regions of an image, we leverage an LLM to provide traversability predictions for each region. This process involves designing prompts that incorporate contextual information about the robot, examples of terrain types, and reference traversability values.

The prompting process begins by describing the robot’s characteristics, such as its size, and mobility characteristics. Additionally, we provide a set of example terrains (e.g., grass, flat terrain, and obstacles) along with their corresponding traversability values as references. These examples help condition the LLM to understand how different terrain features affect traversability for the given robot.

The prompt is then paired with the numbered image generated in the previous step, which is used for asking the LLM to predict a traversability value based on its visual and contextual understanding. The LLM processes this input and outputs a Python list of traversability values, where each position in the list corresponds to a specific region in the image.

### A. Learning a Traversability Distribution

The outputs of the LLMs for traversability predictions can vary across different regions due to the inherent uncertainty in the model’s reasoning and the variability in environmental conditions. To account for this, we model traversability as a latent probabilistic distribution rather than a single deterministic value. This approach allows us to capture both the variability and uncertainty in the predictions, providing a more robust representation of traversability.

Let us consider that the robot is able to query the oracle (in this case, the LLM)  $n \in \mathbb{N}$  times, obtaining  $n$  measurements  $X = \{x_1, x_2, \dots, x_n\}$ . We assume that traversability for each region can be modeled as a Gaussian distribution. However, the oracle can only observe traversability values sampled from the true underlying distribution:

$$x_i \sim \mathcal{N}(m_i, \sigma_i^2), \quad (1)$$

where  $m_i$  and  $\sigma_i^2$  represent the unknown mean and variance of the Gaussian distribution for region  $i$ . The goal is to estimate these parameters,  $m_i$  and  $\sigma_i$ , which define the latent distribution of traversability for each region.

1) *Environment mapping*: Our approach draws inspiration from the counting sensor model for occupancy grid mapping, as outlined in [28] and further explored in [29], [30], [31], [32]. The counting sensor model operates on a discretized grid of map cells, indexed by  $j \in \mathbb{Z}^+$ , and describes the occupancy probability  $\theta_j$  for each cell using a Bernoulli likelihood:

$$p(y_i|\theta_j) = \theta_j^{y_i} (1 - \theta_j)^{1-y_i}, \quad (2)$$

where  $Y = \{y_1, \dots, y_N\}$  represents observations, with  $y_i \in \{0, 1\}$  indicating whether a beam was reflected by ( $y_i = 1$ ) or passed through ( $y_i = 0$ ) the map cell at position  $x_i$ . The positions are given by  $X = \{x_1, \dots, x_N | x_i \in \mathbb{R}^3\}$ . Each range measurement consists of a pair  $(x_i, y_i)$ , and the goal is to compute the posterior distribution of the occupancy probability  $\theta_j$  given the observations  $X$  and  $Y$ .

Using a conjugate Beta prior,  $Beta(\alpha_0, \beta_0)$ , where  $\alpha_0$  and  $\beta_0$  are prior hyperparameters typically chosen as small, uninformative values, we can compute the posterior distribution over  $\theta_j$ . The posterior is given by:

$$p(\theta_j|X, Y) = Beta(\alpha_j, \beta_j), \quad (3)$$

where  $\alpha_j$  and  $\beta_j$  are updated based on the observations. This formulation allows for efficient Bayesian updates and has been widely used in occupancy grid mapping for robotics applications [30].

In our work, we extend this model beyond occupancy estimation by integrating it with traversability assessment. Specifically, we estimate traversability values using a Normal-Inverse-Gamma (NIG) distribution. The NIG distribution provides a flexible framework for handling uncertainty in traversability assessments, particularly in unstructured outdoor environments where sensor noise and terrain variations are prevalent [33], [6].

For each cell, in addition to the occupancy distribution, we model traversability as a random variable with its posterior parameters governed by observations obtained from our

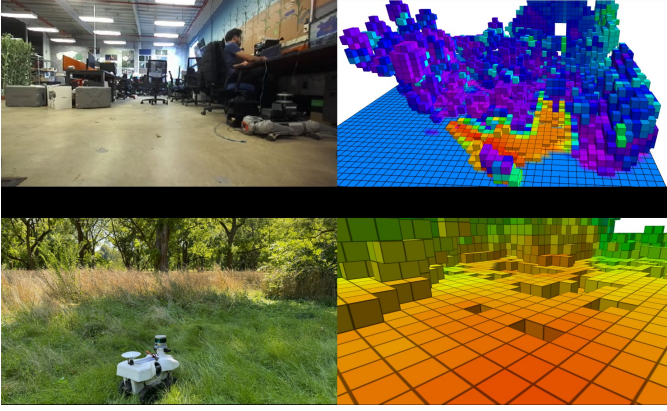


Fig. 4: Example of traversability maps generate using ZeST. The example on top demonstrates a map generate in an indoor environment and the one at the bottom an outdoor environment. Colors towards red represent more traversable terrains.

oracle. The NIG distribution allows us to capture both the mean traversability and its associated uncertainties—aleatoric uncertainty (arising from inherent noise in measurements) and epistemic uncertainty (arising from limited data or model uncertainty)—which are crucial for safe and efficient navigation in challenging conditions.

The Normal-Inverse-Gamma (NIG) distribution is a conjugate prior for the mean  $m$  and variance  $\sigma^2$  of a Gaussian (Normal) distribution. As a conjugate prior, the posterior distribution of  $m$  and  $\sigma^2$ , given observed data, remains within the NIG family. Given observed data  $\{x_1, x_2, \dots, x_n\}$ , the posterior parameters can be obtained as:

$$\begin{aligned} \gamma_n &= \frac{\gamma_0 \kappa_0 + n\bar{x}}{\kappa_n}, & \kappa_n &= \kappa_0 + n, \\ a_n &= a_0 + \frac{n}{2}, & b_n &= b_0 + \frac{1}{2} \sum_{i=1}^n (x_i - \bar{x})^2 + \frac{\kappa_0 n (\bar{x} - \gamma_0)^2}{2(\kappa_0 + n)}, \end{aligned}$$

where  $\bar{x}$  is the sample mean of  $X$ . This Bayesian framework allows us to incorporate both prior knowledge about traversability and observations from LLM outputs into a probabilistic framework. By learning a traversability distribution for each region, we can represent both aleatoric uncertainty (measurement noise) and epistemic uncertainty (limited data).

### B. Risk Assessment

To assess the risk of the robot navigating into a given space, we compute the marginal distribution of  $m$ , which is represented as a Student’s t-distribution [34], [35], where the parameters of the Marginal Student’s t-Distribution are given as

$$s = \underbrace{\sqrt{\frac{b_n(\kappa_n + 1)}{a_n \kappa_n}}}_{\text{Scale}} \cdot \underbrace{\gamma_n}_{\text{Location (Mean)}} \cdot \underbrace{2a_n}_{\text{Degrees of Freedom}}.$$

In the case of ZeST, the traversability map is given as an octomap. Therefore, to compute the CVaR, we take the worst case scenario within each pillar of the map, compressing the z-axis dimension, and generating a grid map. To calculate CVaR

for traversability at a cutoff point  $\alpha$ , we compute the expected value of  $m$  given that  $m$  exceeds its Value at Risk (VaR) at level  $\alpha$ . The VaR at confidence level  $c$  is defined as:

$$\text{VaR}_c = \gamma_n + s \cdot t_{2a,c},$$

where  $t_{2a,c}$  is the  $c$ -quantile of the Student’s t-distribution with  $2a_n$  degrees of freedom.

The CVaR $_c$  is then defined as:

$$\text{CVaR}_c = \mathbb{E}[m \mid m < \text{VaR}_c].$$

For a Student’s t-distribution, CVaR can be computed using:

$$\text{CVaR}_c = \gamma_n - s \cdot \frac{2a + (t_{2a,c})^2}{2a - 1} \cdot \frac{f(t_{2a,c})}{1 - F(t_{2a,c})},$$

where  $f(t_{2a,c})$  is the Probability Density Function (PDF) and  $F(t_{2a,c})$  is the Cumulative Distribution Function (CDF) of the Student’s t-distribution evaluated at  $t_{2a,c}$ .

We precompute the quantiles for different degrees of freedom  $n$  in the range of interest and store these values in a lookup table. For values of  $n$  that fall between precomputed points, we use cubic spline interpolation to approximate the quantile, ensuring efficient and accurate quantile estimation across a wide range of degrees of freedom. This approach avoids the repetitive and costly calculation of quantiles during runtime.

When  $2a$  is large enough, the Student’s t-distribution can be approximated by a Gaussian distribution [34], as the t-distribution converges to the normal distribution  $2a \rightarrow \infty$ . In our implementation, we use  $2a \geq 40$ . In such cases, we switch to using the normal distribution for both quantile and PDF calculations. Employing both solutions, our risk assessment computation achieves a 50x inference speed-up with minimal loss in accuracy.

### C. Traversability-based Path Planning

Based on the current state of the robot, the target pose and the traversability map information, the aim is to find a short and feasible path between the start and the goal pose. Our approach is a motion planner that presents a simplification stage of the planning problem, enabling fast computation of simple solutions while still allowing the planner to navigate more complex paths through tight passages. We utilize the sampling-based RRT algorithm [36] for efficient, rapid planning across long distances. Instead of traditional collision checking, we incorporate our CVaR cost to guide the planner.

1) *Footprint Approximation*: We assess the traversability CVaR of specific robot configurations by modeling their contact areas as rectangles aligned with the robot’s orientation.

The traversability metric for each configuration is determined by the average value of the local CVaR scores of all cells covered by the corresponding pose. To generate the nominal footprint, we approximate the robot’s shape within the planner’s framework by representing it as a rectangle with dimensions equal to half the robot’s size. The pose is given by a position  $(x, y)$  and a heading angle  $(\psi)$ . This simplification allows the robot to rotate in place, facilitating effective planning and navigation in complex environments,

including narrow passages. The rectangular model also simplifies collision checking and footprint generation, reducing the computational overhead without significantly compromising the accuracy of traversability assessments.

2) *Rapidly-exploring Random Tree Star (RRT\*)*: To generate feasible and optimized paths from the robot’s current state to the target pose, we employ a sampling-based Rapidly Exploring Random Tree Star (RRT\*) algorithm [36]. This algorithm operates by incrementally building a tree rooted at the start state and exploring the state space through random sampling.

In the context of traversability-based path planning, RRT\* is adapted to account for the traversability and lambda costs associated with different regions of the environment. Instead of relying solely on collision-free paths, our implementation uses a traversability cost metric that influences the tree expansion and path optimization processes. This ensures that the generated paths are feasible and optimal for the ease of traversal. Therefore, the aim of the path planner to find a short and smooth path with high traversability and lambda, which is reflected in the cost function.

The total cost  $c$  for a path segment connecting state  $n = (x, y, \psi)$  and its adjacent state  $n' = (x', y', \psi')$  is comprised of the segment’s traversability CVaR  $c_{CVaR}$  and the epistemic uncertainty measurement given by  $n$  with cost  $c_n$ .

$$c = c_{CVaR} + c_n$$

Incorporating  $c_{CVaR}$  into the cost function ensures that the planner is guided to favor routes that are safer and easier for the robot to navigate. The traversability cost is given by

$$c_{CVaR} = e^{-w_1 \cdot CVaR(x_i)}$$

where  $w_1$  is the respective weight and  $CVaR(x_i)$  represents the evaluated CVaR value at state  $x_i$  given all the grid cells covered by the robot’s footprint. Additionally, by using  $c_\kappa$ , the planner accounts for environmental uncertainty and preferentially selects areas that have been most frequently observed. To compute the  $c_\kappa$  cost, we have

$$c_\kappa = w_2 \cdot e^{\kappa_b - \kappa(x_i)}$$

with  $w_2$  as a weighting parameter that controls the influence of the confidence level on the overall cost and  $\kappa(x_i)$  denotes the evaluate count value for all the grid cells covered by the robot’s footprint.  $\kappa_b$  is a bias term to ensure that the argument of the exponential function maintains meaningful scaling of the confidence levels, allowing the planner to effectively penalize path segments with lower confidence values.

Furthermore, we do not incorporate an explicit distance cost in our objective function. This omission is intentional, as longer paths inherently accumulate higher traversability and lambda costs. Consequently, the cost function implicitly favors shorter routes without the need for a separate distance penalty.

#### D. Traversability-based Model Predictive Controller

To control the robot and guide it towards a defined reference, we use sampling-based model predictive control, more specifically the Model Predictive Path Integral (MPPI) [37].

We design a model predictive controller with a optimization horizon  $N \in \mathbb{N}$ . Similar to the path planner used in Section III-C, we use the footprint approximation to get the CVaR values and counts from the predicted gridmap. With such values, the sampling-based MPC samples random actions and minimizes the a cost function defined in Eq. (4). The resulting finite-horizon optimization problem is formulated as

$$\min_{x_k, u_k} \sum_{i=k}^{k+N-1} (\|x_i - x_i^r\|_Q^2 + \mathcal{J}_{k,u}) + \|x_{k+N} - x_{k+N}^r\|_Q^2 - \sum_{i=k}^{k+N} W_1 \cdot CVaR(x_i), \quad (4)$$

where the first term minimizes the error between the predicted states  $x_i$  and the reference states  $x_i^r$  along the path, ensuring accurate tracking, the second term minimizes the difference in the predicted actions, limiting the action space, the third term minimizes the terminal cost, driving the robot toward the goal location, and the fourth maximizes CVaR over traversability predictions to prioritize safety.

---

#### Algorithm 1: RRT Algorithm for Traversability-Aware Path Planning

---

**Require:** Start state  $x_{start}$ , Goal state  $x_{goal}$ , State space bounds  $\mathcal{X}$ , Traversability map  $T$ , Cost weights  $\alpha_1, \alpha_2$ , Maximum iterations  $N$ , Step size  $\delta$ , Rewire radius  $r$

Initialize tree  $\mathcal{T}$  with root node  $x_{start}$

**for**  $i = 1$  **to**  $N$  **do**

    Sample random state  $x_{rand} \leftarrow \text{Sample}(\mathcal{X})$

    Find nearest node  $x_{nearest} \leftarrow \text{Nearest}(\mathcal{T}, x_{rand})$

$x_{new} \leftarrow \text{Steer}(x_{nearest}, x_{rand}, \delta)$

**if**  $isValid(x_{new}, T)$  **then**

        Find nearby nodes  $\mathcal{N} \leftarrow \text{Near}(\mathcal{T}, x_{new}, r)$

$x_{min} \leftarrow \arg \min_{x \in \mathcal{N}} (J(x_{start}, x) + J(x, x_{new}))$

        Add  $x_{new}$  to  $\mathcal{T}$  with parent  $x_{min}$

**for each**  $x_{near}$  **in**  $\mathcal{N}$  **do**

**if**  $J(x_{start}, x_{new}) + J(x_{new}, x_{near}) < J(x_{start}, x_{near})$

**then**

                    Rewire( $x_{near} \rightarrow x_{new}$ )

**end**

**end**

**if**  $isGoalReached(x_{new}, x_{goal})$  **then**

            Extract path

$\pi \leftarrow \text{ExtractPath}(\mathcal{T}, x_{start}, x_{goal})$

**Return** path

**end**

**end**

**end**

**Return** Best path found

---

For ZeST, we design a speed-conditioned epistemic uncertainty cost, where the desired speed is changed according to the uncertainty attributed to that predictive path. Since traversability is predicted using a counting model, as more measurements are gathered from a space, the lower the epistemic uncertainty will be in that corresponding area. Therefore, we want the robot to navigate slower on areas where the

uncertainty is high, such that it has more time to learn the true distribution of that location. For such, we incorporate an action cost where  $\mathcal{J}_{i,u} = \|u_i - u_i^r \cdot (1 - e^{(n_0 - n_i) \cdot W_2})\|_R$ .

$Q$ ,  $Q_N$ , and  $W_1$  are weights that balance each component of the cost function. After minimizing the cost function, the first command in the control horizon is used to drive the robot towards the goal.

#### IV. EXPERIMENTAL RESULTS

In this section, we present the implementation of ZeST in the real world and analyze the experimental results.

##### A. Implementation

We implemented ZeST on the TerraSentia robot, a small light weight skid-steer robot manufactured by Earthsense Inc. The robot comes equipped with a 6 DOF IMU, Global Navigation Satellite System (GNSS), and wheel encoders. In addition we equipped it with a Velodyne VLP16 LiDAR for 3d point cloud, and a Jetson AGX for onboard computation. We also installed a GSM router for online GPT-4o API calls.

##### B. Baseline Methods

We compare ZeST against several existing methods for both indoor and outdoor navigation.

- 1) NoMaD [38]: A foundation model for visual navigation that uses a Transformer policy and diffusion based encoder trained on diverse robotic navigation datasets to perform goal-conditioned and goal-agnostic navigation.
- 2) CoNVOI [17]: A Vision Language Model (VLM) based method that generates context-aware trajectories by identifying robot environment, implicit and explicit navigation behaviors.

##### C. Navigation in real unstructured environments

Method	Indoor	Outdoor
NoMaD	5/10	3/5
CoNVOI	3/10	2/5
<b>ZeST(Ours)</b>	10/10	5/5

TABLE I: Summary of Navigation Runs (successful runs/total runs) in challenging indoor and outdoor environment.

In this section, we evaluate the performance of our model against other navigation methods: NoMaD and CoNVOI. Table I and Fig. 5 provide a summary of the navigation runs across two different environments. The goal of the experiments is zero shot navigation to a specified goal location. ZeST demonstrated superior performance in zero shot setting and outperforms both baselines in all environments.

In the first environment, the robot navigates to the goal in an indoor cluttered environment. Ten repetitions were conducted for each method, with the robot starting from the same initial location. The objective is to reach the target located behind multiple obstacles, with only one viable path available with no trivial solutions. ZeST built a traversability map on the fly and generated paths through the highly traversable areas. As can

be seen in Fig. 5 ZeST paths are located in the lighter regions which represent highly traversable areas whereas the darker blue regions represent untraversable or low traversability areas. In contrast, NoMAD tested in the zero shot manner, reached the goal successfully only half of the time, demonstrating that despite being a foundational method trained on a large dataset with diverse environments and robotic platforms, it failed to generalize effectively in a zero-shot scenario. CoNVOI similar to our method uses an LLM like GPT-4o, however it queries the LLM to chose between possible navigation paths for a given scenario. We change the behavior prompt to select paths that are traversable and obstacle free which is different than the original prompt like: selecting paths on the right side of corridor to mimic human behavior. In the indoor cluttered environment, CoNVOI only reaches the goal three times, as the LLM sees no obstacle free path in all possible paths and hence picks the path that is closest to its navigation behavior prompts.

In the second environment, the robot navigates to the goal in a forest like environment with 5 repetitions. ZeST with its VLM based scene understanding is able to provide accurate traversability scores leading to successful navigation in each run. NoMaD performs slightly better in the outdoor environment reaching the goal three times but relies on navigation behaviors learned during training for zero shot navigation leading to failures. NoMaD requires fine tuning to reliably perform in a new environment. CoNVOI still struggles to navigate to the goal and only does so two times. We believe that with our modified prompt the method struggles to find a good reference path to follow.

##### D. Latency Analysis

A key factor in the real-time performance of ZeST is the latency introduced by querying large multi-modal LLMs. Fig. 6 illustrates the distribution of latency measurements when GPT-4o is queried, averaged over multiple runs. The histogram shows that majority of the queries take about 1-2.5 seconds with occasional outliers taking up to 5 seconds.

To address this, at each time step our system uses the LLM prediction to generate an Octomap that can predict 10 meters away from the robot. This allows the robot to query the LLM and update the map until it reaches the border of the map. We also set up a cost in the model predictive controller which slows down the robot in unknown areas. Using the epistemic uncertainty modeled in the map, the cost balances the exploration of new unknown areas and known untraversable areas. It also gives the robot time to query the LLM and improve safety in unknown areas.

Another key factor for ZeST is segmentation which is done using off the shelf models like SAM or SLIC. SAM is a state-of-the-art segmentation model which can generate masks automatically by sampling prompts across the image [26]. SAM leverages a robust image encoder combined with prompt-based interaction mechanisms (e.g., key points or bounding boxes) to produce high-quality segmentation masks. SLIC (Simple Linear Iterative Clustering) on the other hand is an efficient superpixel generation algorithm that clusters pixels

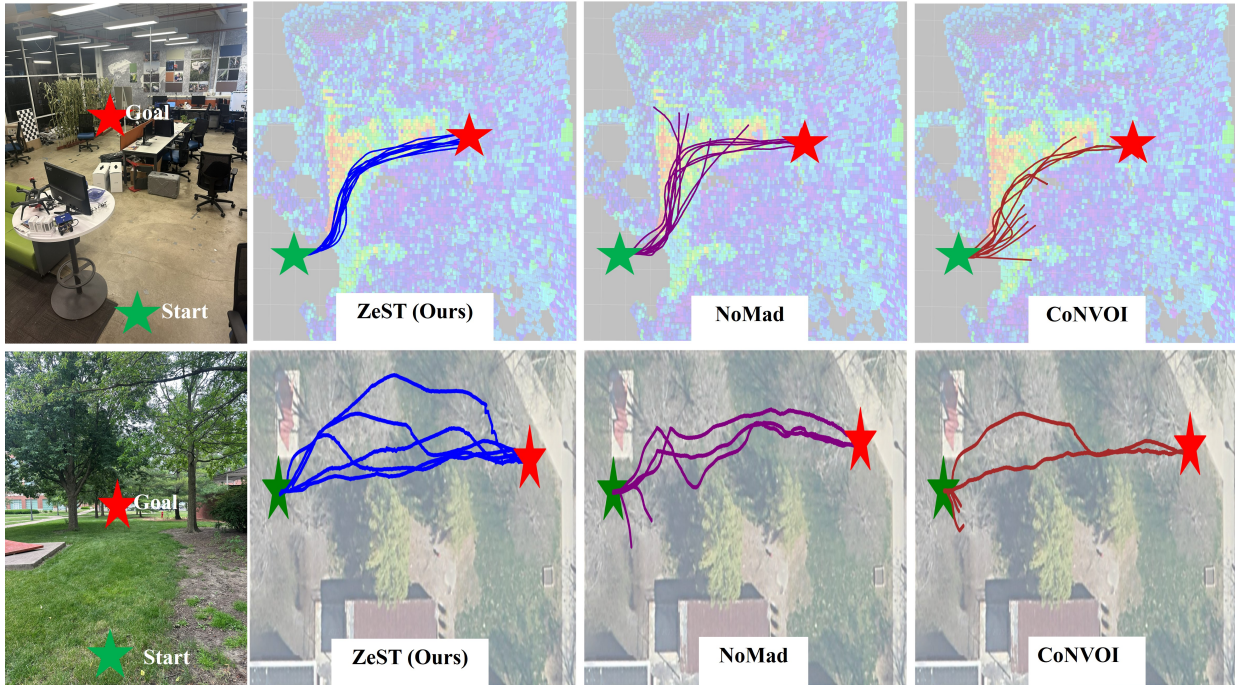


Fig. 5: Visualization of ZeST deployed in challenging environments compared to NoMaD and CoNVOI. The top row shows the indoor experiment plotted on the traversability octomap created by ZeST. The bottom row show the outdoor experiment plotted on the top down view of the scene.

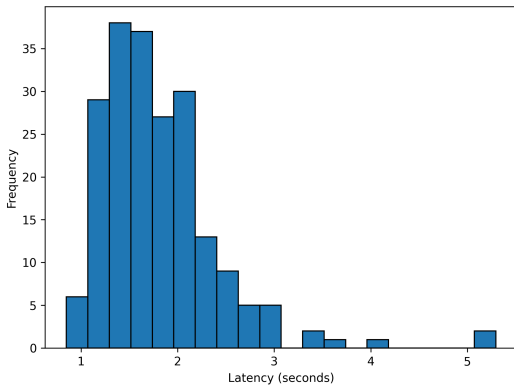


Fig. 6: Histogram of latency.

based on both color similarity and spatial proximity in a five-dimensional space (Lab color space and pixel coordinates) [27]. Unlike traditional k-means clustering, SLIC reduces computational complexity by limiting the search space for each cluster center to a region proportional to the superpixel size.

We compare both models as seen in Fig. 7 the segmentation masks generated by SAM and SLIC are different. The masks generated by SAM correspond to objects and surfaces whereas the masks from SLIC divide the image into regions based on proximity and color. Even so, when the masks are numbered to create visual markers that the LLM can use for grounding the markings are similar. This leads to same response generated from the LLM. However, looking at run time for both methods, we notice that SLIC due to its simpler algorithm takes on average 0.1 second per image whereas SAM takes 1 second. Hence, we use SLIC as the mask generation model for real

time deployment.

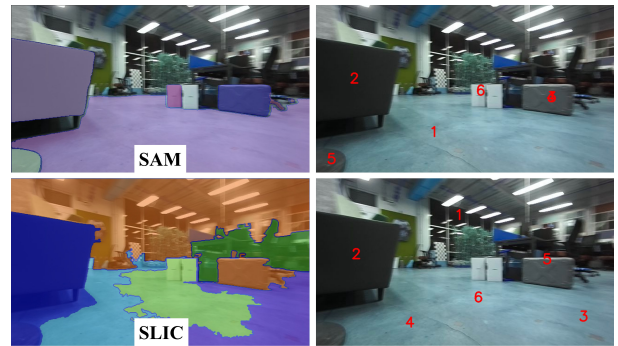


Fig. 7: Comparison of SAM (Top row) and SLIC (Bottom row) methods for visual marking.

## V. CONCLUSION

In this work we demonstrated ZeST, a navigation method that leverages multi-modal LLMs to create global traversability maps. The method operates in a zero-shot manner, eliminating the need for robots to experience dangerous areas to learn their traversability representation. Since the generated map is global, it enables the use of global path planning for long-term autonomous navigation, while a short-term sampling-based model predictive controller (MPC) is used for fast and reactive local planning.

As demonstrated, the generated maps are consistent with real-world environments, providing reliable traversability predictions that enhance navigation safety and efficiency. Moreover, the proposed pipeline achieves better navigational performance compared to state-of-the-art foundational models designed for navigation tasks, bridging multi-modal LLMs into

robotic systems to improve both understanding of complex environments and overall autonomy.

## REFERENCES

- [1] M. V. Gasparino, A. N. Sivakumar, Y. Liu, A. E. Velasquez, V. A. Higuti, J. Rogers, H. Tran, and G. Chowdhary, "Wayfast: Navigation with predictive traversability in the field," *IEEE Robotics and Automation Letters*, vol. 7, no. 4, pp. 10651–10658, 2022.
- [2] M. V. Gasparino, A. N. Sivakumar, and G. Chowdhary, "Wayfaster: a self-supervised traversability prediction for increased navigation awareness," *arXiv preprint arXiv:2402.00683*, 2024.
- [3] S. Gummadi, M. V. Gasparino, D. Vasisht, and G. Chowdhary, "Fed-ec: Bandwidth-efficient clustering-based federated learning for autonomous visual robot navigation," *IEEE Robotics and Automation Letters*, 2024.
- [4] X. Cai, S. Ancha, L. Sharma, P. R. Osteen, B. Bucher, S. Phillips, J. Wang, M. Everett, N. Roy, and J. P. How, "Evora: Deep evidential traversability learning for risk-aware off-road autonomy," *arXiv preprint arXiv:2311.06234*, 2023.
- [5] J. Frey, M. Mattamala, N. Chebrolov, C. Cadena, M. Fallon, and M. Hutter, "Fast traversability estimation for wild visual navigation," *arXiv preprint arXiv:2305.08510*, 2023.
- [6] M. Wermelinger, P. Fankhauser, R. Diethelm, P. Krüsi, R. Siegwart, and M. Hutter, "Navigation planning for legged robots in challenging terrain," in *2016 IEEE/RSJ International Conference on Intelligent Robots and Systems (IROS)*. IEEE, 2016, pp. 1184–1189.
- [7] G. Kahn, P. Abbeel, and S. Levine, "Badgr: An autonomous self-supervised learning-based navigation system," *IEEE Robotics and Automation Letters*, vol. 6, no. 2, pp. 1312–1319, 2021.
- [8] A. N. Sivakumar, S. Modi, M. V. Gasparino, C. Ellis, A. E. B. Velasquez, G. Chowdhary, and S. Gupta, "Learned visual navigation for under-canopy agricultural robots," in *17th Robotics: Science and Systems, RSS 2021*. MIT Press Journals, 2021.
- [9] A. N. Sivakumar, M. V. Gasparino, M. McGuire, V. A. Higuti, M. U. Akcal, and G. Chowdhary, "Lessons from deploying cropfollow++: Under-canopy agricultural navigation with keypoints," *arXiv preprint arXiv:2404.17718*, 2024.
- [10] V. S. Dorbala, G. Sigurdsson, R. Piramuthu, J. Thomason, and G. S. Sukhatme, "Clip-nav: Using clip for zero-shot vision-and-language navigation," *arXiv preprint arXiv:2211.16649*, 2022.
- [11] M. Ahn, A. Brohan, N. Brown, Y. Chebotar, O. Cortes, B. David, C. Finn, C. Fu, K. Gopalakrishnan, K. Hausman *et al.*, "Do as i can, not as i say: Grounding language in robotic affordances," *arXiv preprint arXiv:2204.01691*, 2022.
- [12] N. M. M. Shafiqullah, C. Paxton, L. Pinto, S. Chintala, and A. Szlam, "Clip-fields: Weakly supervised semantic fields for robotic memory," *arXiv preprint arXiv:2210.05663*, 2022.
- [13] D. Shah, B. Osiński, S. Levine *et al.*, "Lm-nav: Robotic navigation with large pre-trained models of language, vision, and action," in *Conference on robot learning*. PMLR, 2023, pp. 492–504.
- [14] P. Chen, X. Sun, H. Zhi, R. Zeng, T. H. Li, G. Liu, M. Tan, and C. Gan, "A<sup>2</sup>nav: Action-aware zero-shot robot navigation by exploiting vision-and-language ability of foundation models," *arXiv preprint arXiv:2308.07997*, 2023.
- [15] C. Huang, O. Mees, A. Zeng, and W. Burgard, "Visual language maps for robot navigation," in *2023 IEEE International Conference on Robotics and Automation (ICRA)*. IEEE, 2023, pp. 10608–10615.
- [16] P. Liu, Y. Orru, J. Vakil, C. Paxton, N. M. M. Shafiqullah, and L. Pinto, "Ok-robot: What really matters in integrating open-knowledge models for robotics," *arXiv preprint arXiv:2401.12202*, 2024.
- [17] A. J. Sathyamoorthy, K. Weerakoon, M. Elnoor, A. Zore, B. Ichter, F. Xia, J. Tan, W. Yu, and D. Manocha, "Convoi: Context-aware navigation using vision language models in outdoor and indoor environments," in *2024 IEEE/RSJ International Conference on Intelligent Robots and Systems (IROS)*. IEEE, 2024, pp. 13837–13844.
- [18] T. Brown, B. Mann, N. Ryder, M. Subbiah, J. D. Kaplan, P. Dhariwal, A. Neelakantan, P. Shyam, G. Sastry, A. Askell *et al.*, "Language models are few-shot learners," *Advances in neural information processing systems*, vol. 33, pp. 1877–1901, 2020.
- [19] H. Touvron, L. Martin, K. Stone, P. Albert, A. Almahairi, Y. Babaei, N. Bashlykov, S. Batra, P. Bhargava, S. Bhosale *et al.*, "Llama 2: Open foundation and fine-tuned chat models," *arXiv preprint arXiv:2307.09288*, 2023.
- [20] J. Achiam, S. Adler, S. Agarwal, L. Ahmad, I. Akkaya, F. L. Aleman, D. Almeida, J. Altenschmidt, S. Altman, S. Anadkat *et al.*, "Gpt-4 technical report," *arXiv preprint arXiv:2303.08774*, 2023.
- [21] H. Liu, C. Li, Q. Wu, and Y. J. Lee, "Visual instruction tuning," *Advances in neural information processing systems*, vol. 36, pp. 34892–34916, 2023.
- [22] G. Team, R. Anil, S. Borgeaud, Y. Wu, J. Alayrac, J. Yu, R. Soricut, J. Schalkwyk, A. Dai, A. Hauth *et al.*, "Gemini: A family of highly capable multimodal models, 2024," *arXiv preprint arXiv:2312.11805*, 2024.
- [23] H. Liu, C. Li, Y. Li, and Y. J. Lee, "Improved baselines with visual instruction tuning," in *Proceedings of the IEEE/CVF Conference on Computer Vision and Pattern Recognition*, 2024, pp. 26296–26306.
- [24] A. Liu, B. Feng, B. Xue, B. Wang, B. Wu, C. Lu, C. Zhao, C. Deng, C. Zhang, C. Ruan *et al.*, "Deepseek-v3 technical report," *arXiv preprint arXiv:2412.19437*, 2024.
- [25] H. Lu, W. Liu, B. Zhang, B. Wang, K. Dong, B. Liu, J. Sun, T. Ren, Z. Li, H. Yang *et al.*, "Deepseek-v1: towards real-world vision-language understanding," *arXiv preprint arXiv:2403.05525*, 2024.
- [26] N. Ravi, V. Gabeur, Y.-T. Hu, R. Hu, C. Ryal, T. Ma, H. Khedr, R. Rädle, C. Rolland, L. Gustafson *et al.*, "Sam 2: Segment anything in images and videos," *arXiv preprint arXiv:2408.00714*, 2024.
- [27] R. Achanta, A. Shaji, K. Smith, A. Lucchi, P. Fua, and S. Süsstrunk, "Slic superpixels compared to state-of-the-art superpixel methods," *IEEE transactions on pattern analysis and machine intelligence*, vol. 34, no. 11, pp. 2274–2282, 2012.
- [28] D. Hahnel, R. Triebel, W. Burgard, and S. Thrun, "Map building with mobile robots in dynamic environments," in *2003 IEEE International Conference on Robotics and Automation (Cat. No. 03CH37422)*, vol. 2. IEEE, 2003, pp. 1557–1563.
- [29] S. Thrun, "Learning occupancy grid maps with forward sensor models," *Autonomous robots*, vol. 15, pp. 111–127, 2003.
- [30] K. Doherty, T. Shan, J. Wang, and B. Englot, "Learning-aided 3-d occupancy mapping with bayesian generalized kernel inference," *IEEE Transactions on Robotics*, vol. 35, no. 4, pp. 953–966, 2019.
- [31] L. Gan, R. Zhang, J. W. Grizzle, R. M. Eustice, and M. Ghaffari, "Bayesian spatial kernel smoothing for scalable dense semantic mapping," *IEEE Robotics and Automation Letters*, vol. 5, no. 2, pp. 790–797, 2020.
- [32] J. Kim, J. Seo, and J. Min, "Evidential semantic mapping in off-road environments with uncertainty-aware bayesian kernel inference," *arXiv preprint arXiv:2403.14138*, 2024.
- [33] A. Chilian and H. Hirschmüller, "Stereo camera based navigation of mobile robots on rough terrain," in *2009 IEEE/RSJ International Conference on Intelligent Robots and Systems*. IEEE, 2009, pp. 4571–4576.
- [34] D. C. Montgomery and G. C. Runger, *Applied statistics and probability for engineers*. John Wiley & sons, 2010.
- [35] K.-R. Koch, *Introduction to Bayesian statistics*. Springer Science & Business Media, 2007.
- [36] S. Karaman, M. R. Walter, A. Perez, E. Frazzoli, and S. Teller, "Anytime motion planning using the rrt," in *2011 IEEE international conference on robotics and automation*. IEEE, 2011, pp. 1478–1483.
- [37] G. Williams, N. Wagener, B. Goldfain, P. Drews, J. M. Reh, B. Boots, and E. A. Theodorou, "Information theoretic mpc for model-based reinforcement learning," in *2017 IEEE International Conference on Robotics and Automation (ICRA)*. IEEE, 2017, pp. 1714–1721.
- [38] A. Sridhar, D. Shah, C. Glossop, and S. Levine, "Nomad: Goal masked diffusion policies for navigation and exploration," *arXiv preprint arXiv:2310.07896*, 2023.